JOURNAL OF BIOMOLECULAR STRUCTURE AND DYNAMICS
https://doi.org/10.1080/07391102.2021.1994013

Taylor & Francis
Taylor & Francis Group

RESEARCH ARTICLE

Celecoxib, Glipizide, Lapatinib, and Sitagliptin as potential suspects of aggravating SARS-CoV-2 (COVID-19) infection: a computational approach

Mohamed F. AlAjmi, Md Tabish Rehman and Afzal Hussain

Department of Pharmacognosy, College of Pharmacy, King Saud University, Riyadh, Saudi Arabia

Communicated by Ramaswamy H. Sarma

ABSTRACT

COVID-19 caused by SARS-CoV-2 has emerged as a potential threat to human life, especially to people suffering from chronic diseases. In this study, we investigated the ability of selected FDA-approved drugs to inhibit TACE (tumor necrosis factor α converting enzyme), which is responsible for the shedding of membrane-bound ACE2 (angiotensin-converting enzyme2) receptors into soluble ACE2. The inhibition of TACE would lead to an increased population of membrane-bound ACE2, which would facilitate ACE2-Spike protein interaction and viral entry. A total of 50 drugs prescribed in treating various chronic diseases in Saudi Arabia were screened by performing molecular docking using AutoDock4.2. Based on docking energy (≤ -9.00 kcal mol^{-1}), four drugs (Celecoxib, Glipizide, Lapatinib, and Sitagliptin) were identified as potential inhibitors of TACE, with binding affinities up to 10^6–10^7 M^{-1}. Analysis of the molecular docking suggests that these drugs were bound to TACE's catalytic domain and interact with the key residues such as His405, Glu406, and His415, which are involved in active site Zn^{2+} ion chelation. Molecular dynamics simulation was performed to confirm the stability of TACE-drugs complexes. RMSD (root mean square deviation), RMSF (root mean square fluctuation), Rg (radius of gyration), and SASA (solvent accessible surface area) were within the acceptable limits. Free energy calculations using Prime-MM/GBSA suggest that Celecoxib formed the most stable complex with TACE, followed by Glipizide, Sitagliptin, and Lapatinib. The finding of this study suggests a mechanism for drugs to aggravate SARS-CoV-2 infection and hence high mortality in patients suffering from chronic diseases.

ARTICLE HISTORY
Received 12 March 2021
Accepted 11 October 2021

KEYWORDS
SARS-CoV-2; Coronavirus; ADAM17; molecular docking and simulation; chronic diseases; COVID-19 activation

1. Introduction

The emergence of the SARS-CoV-2 pandemic is a worldwide threat to public health and the economy. SARS-CoV-2 originated from wild bats and belongs to group 2 of beta-coronaviruses, which also contains SARS-CoV. Genome-wide analysis revealed that SARS-CoV-2 shares only 70% genome similarity with another member of the same group, i.e. SARS-CoV (Gralinski & Menachery, 2020; She et al., 2020). The first SARS-CoV-2 (COVID-19) case with pneumonia-like symptoms was reported in the Huanan seafood market, Wuhan, Hubei, China, on Dec 12, 2019 (Zhou et al., 2020). Since then, it has spread over the whole world and caused more than 74 million confirmed cases and the deaths of over 1.6 million patients. The genetic material of SARS-CoV-2 is a 29.9 kb long (+) RNA molecule wrapped around by nucleocapsid protein (N). The RNA + N protein forms the core of the virus, surrounded by envelope protein (E), membrane protein (M), and spike protein (S) in a lipid bilayer membrane. SARS-CoV-2 encodes 14 open reading frames (ORFs), encoding 27 proteins (Lu et al., 2020). The 5′ end of the genome contains ORFs 1a and 1ab, while the 3′ end of the genome consists of 4 structural proteins (S, E, M, and N) and 8 accessory proteins such as 3a, 3 b, p6, 7a, 7 b, 8 b, 9 b and orf14. The polypeptide pp1a (produced by ORF1a) contains two viral proteases, namely papain-like protease (PLpro) and 3 C-like protease (3CLpro). These proteases further cleave polypeptides pp1a and pp1ab into 15 functional nonstructural proteins (nsps) from nsp1 to nsp10 and from nsp12 to nsp16. The nsps play essential roles in the replication process of the virus. Some of the nsps are single-stranded RNA binding protein (nsp9), growth factor-like protein (nsp10), viral RNA-dependent RNA polymerase (nsp12), RNA helicase (nsp13), exo-ribonuclease (nsp14), endo-ribonuclease (nsp15), and 2′-O-ribose methyltransferase (nsp16).

SARS-CoV-2 gains entry into the host cell through an interaction between Spike protein and host angiotensin-converting enzyme 2 (ACE2) receptor. Spike protein comprises a signal peptide at the N-terminal end (1-13 aa), S1 subunit (14-685 aa), and S2 subunit (686-1273 aa). The S1 subunit can further be classified into an N-terminal domain (NTD; 14-305 aa) and a receptor-binding domain (RBD; 319-541 aa). Similarly, the S2 subunit can be categorized into a fusion peptide (788-806 aa), heptapeptide repeats (HR1; 921-984 aa, and HR2; 1163-1213 aa), transmembrane domain (TM: 1214-

CONTACT Md Tabish Rehman mrehman@ksu.edu.sa Department of Pharmacognosy, College of Pharmacy, King Saud University, Riyadh 11451, Saudi Arabia

1237 aa), and a cytoplasmic domain (CPD; 1238-1273 aa). The S1 and S2 subunits of SARS-CoV-2 participate in recognizing ACE2 receptor protein and the virus's fusion to the host membrane, respectively (Lan et al., 2020). ACE2, a metallo-carboxypeptidase expressed on the host's cell surface, is responsible for the maturation of human angiotensin (Ang). ACE2 cleaves Ang II into Ang (1-7) and Ang I into Ang (1-9), thereby precluding Ang I into Ang II conversion. There are two domains, an N-terminal peptidase domain (PD) and a C-terminal collectrin-like domain (CLD), in a mature ACE2 receptor. The PD domain of ACE2 recognizes the RBD of Spike protein S1 domain, thereby bringing HR1 and HR2 of the Spike protein S2 domain in close proximity to form a six-helix bundle (6-HB) fusion core. The fusion core facilitates the merging of viral and host cell membranes, and thus, the virus's internalization (Luan et al., 2020). An interaction of Spike protein with ACE2 elicits conformational changes in the Spike protein, enhancing its sensitivity to proteolytic cleavage by TMPRSS2 (transmembrane serine protease 2) and clathrin-dependent endocytosis (Hoffmann et al., 2020; Wu et al., 2020). SARS-CoV-2 infection often results in the downregulation of ACE2, which might be due to the shedding of membrane-bound ACE2 into soluble ACE2 by ADAM17 (a disintegrin and metalloprotease 17) or TACE (TNF-α converting enzyme). The function of two proteases, namely TMPRSS2 and ADAM17 or TACE, is antagonistic, i.e. they compete for ACE2 cleavage. TMPRSS2 cleaves the intracellular tail of ACE2, while ADAM17 or TACE is responsible for ACE2 ectodomain shedding (Heurich et al., 2014). It is worth noting that soluble ACE2 has a high affinity towards SARS-CoV-2 and can directly neutralize the virus. Reports suggest that recombinant human ACE2 (rhACE2) can mimic soluble ACE2 and thus inhibit viral infection by competing with membrane-bound ACE2 receptors (Monteil et al., 2020). Therefore, in addition to its absolute expression, the cleavage and shedding of ACE2 could influence COVID-19 entry into cells (Palau et al., 2020).

Recent reports suggest that patients suffering from chronic diseases such as diabetes, hypertension, kidney disease, arthritis, asthma, and cancer are at higher risk of contracting severe COVID-19 (Zipeto et al., 2020). In the present study, we have utilized computational approaches to evaluate the hypothesis that FDA-approved drugs that treat chronic diseases can bind and inhibit TACE or ADAM17. This would lead to an increased number of membrane-bound ACE2 receptors, an entry point of SARS-CoV-2.

2. Material and methods

2.1. Selection of drugs and their preprocessing

The FDA-approved drugs commonly used in Saudi Arabia were searched in the literature and selected for this study (Table 1). These drugs are prescribed to treat different chronic diseases such as cancer, diabetes, arthritis, neurodegeneration, and asthma. The 2 D structure of 50 drugs was retrieved from PubChem and preprocessed before molecular docking by removing any salt, merging non-polar hydrogen atoms, assigning bond orders, defining rotatable bonds, adding Gasteiger partial charges using AutoDock tools, as defined previously (Rehman et al., 2014). The energy of drugs was minimized using a universal force field (UFF) and conjugate optimization algorithm with 200 steps.

Table 1. List of FDA-approved medication commonly used in Saudi Arabia for the treatment of different chronic diseases.

S. no.	Categories of medications	PubChem CID	Name of drugs
1.	*Anticancer*	148124	Docetaxel
2.		22420	Cyclophosphamide
3.		41867	Epirubicin
4.		3385	Fluorouracil
5.		426756	Carboplatin
6.		31703	Doxorubicin
7.		36314	Paclitaxel
8.		60953	Capecitabine
9.		5702198	Cisplatin
10.		5311497	Vinorelbine
11.		3902	Letrozole
12.		2733526	Tamoxifen
13.		104741	Fulvestrant
14.		387447	Bortezomib
15.		208908	Lapatinib
16.		176870	Erlotinib
17.		3005573	Toremifene
18.	*Antidiabetic*	4091	Metformin
19.		3475	Gliclazide
20.		3488	Glibenclamide
21.		3476	Glimepiride
22.		3478	Glipizide
23.		71793	Glyclopyramide
24.		4369359	Sitagliptin
25.		6918537	Vildagliptin
26.		11243969	Saxagliptin
27.		10096344	Linagliptin
28.		4829	Pioglitazone
29.		77999	Rosiglitazone
30.		41774	Acarbose
31.		65981	Repaglinide
32.		45588096	Exenatide
33.		16134956	Liraglutide
34.		16131098	Insulin
35.	*Anti-arthritis*	3672	Ibuprofen
36.		3033	Diclofenac
37.		3715	Indomethacin
38.		4044	Mefenamic acid
39.		1548887	Sulindac
40.		2662	Celecoxib
41.		54677470	Meloxicam
42.		156391	Naproxene
43.	*Anti-alzheimer*	3152	Donepezil
44.		77991	Rivastigmine
45.		9651	Galantamine
46.		4045	Memantine
47.	*Anti-asthma*	5311101	Fluticasone
48.		5281004	Budesonide
49.		82153	Flunisolide
50.		6918155	Ciclesonide

2.2. Identification of target protein and its preprocessing

The 3 D coordinates of protein i.e. TACE or ADAM17 (PDB ID: 3B92; resolution 2.00 Å) were downloaded from the RCSB database (https://www.rcsb.org/structure/3B92). The X-ray crystal structure of TACE reports a thiol-containing aryl sulfone as a potent inhibitor. The cognate inhibitor was identified as 3-{[4-(but-2-yn-1-yloxy)phenyl]sulfonyl}propane-1-thiol (Bandarage et al., 2008). Before molecular docking, TACE's structure was preprocessed by deleting

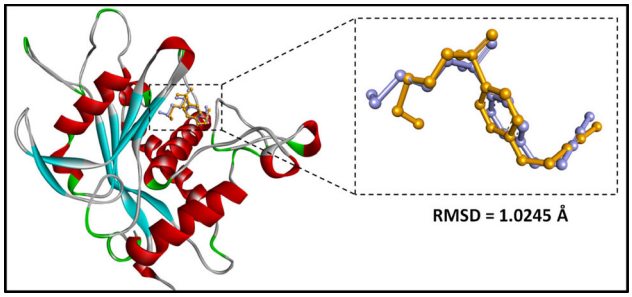

Figure 1. Validation of molecular docking protocol by re-docking the ligand and comparing the RMSD between the re-docked pose and crystal structure pose. The re-docked pose and crystal structure pose of the ligand are shown in purple and golden colors, respectively.

crystallographic water molecules and any other hetero-molecule, including the bound inhibitor. The missing hydrogen atoms were added, Kollman united atom type charges were assigned, and a new network of hydrogen bonds was created. The energy of the complete system was minimized by the Merck molecular force field (MMFF). A grid of $28.1 \times 23.3 \times 25.9$ Å centered at $0.21 \times 62.2 \times 86.1$ Å with 0.375 Å spacing was created by AutoGrid (Morris et al., 2009).

2.3. Molecular docking

The interaction between protein and drug was ascertained by performing molecular docking in AutoDock4.2, as reported earlier (Al-Yousef et al., 2017; Morris et al., 2009). Default AutoDock parameters were used, and the distance-dependent dielectric functions were employed to enumerate van der Waals' and electrostatic parameters. Docking was performed using a Lamarck Genetic Algorithm (LGA) and the Solis and Wets local search methods (Solis & Wets, 1981). The ligand's initial position, orientation, and torsions were set randomly, and all the rotatable torsions were relaxed. A total of 10 docking runs were performed for each ligand, and a maximum of 2.5×10^6 energy calculations recorded for each docking run. The population size, translational step, quaternions, and torsions were set to 150, 0.2 Å, 5, and 5, respectively. The results were analyzed in Discovery Studio2.5 (Accelrys). The binding affinity (K_d) of the ligand towards protein was calculated from its binding energy (ΔG) using the relation (Khan et al., 2020; Rabbani et al., 2018):

$$\Delta G = -RT \ln K_d$$

where R and T are the universal gas constant and temperature, respectively.

2.4. Molecular dynamics (MD) simulation

Molecular dynamics (MD) simulation is a widely employed method to evaluate a protein-ligand complex's stability and dynamics. MD simulation of protein-ligand complexes were performed in triplicates using Desmond (Schrodinger, LLC, NY, USA), as described earlier (AlAjmi et al., 2018; Rehman et al., 2019). The energy minimized protein-ligand complex was placed in an orthorhombic box and solvated with TIP3P water molecules. The buffer region between the complex and the boundaries of simulation was set at 1 nm. The system was neutralized by adding proper counterions, and the physiological conditions were maintained by adding 0.15 mM NaCl. The energy of the system was minimized using Optimized Parameters for Liquid Simulations (OPLS3a) force-field. The protein-drug system's energy was minimized using a five step relaxation protocol: (i) Brownian dynamics in an NVT ensemble for 100 ps at 10 K with small time-steps and restraints on solute heavy atoms, (ii) a 12 ps simulation under an NVT ensemble at 10 K (thermostat relaxation = 0.1 ps) and pressure 1 atm (barostat relaxation = 50 ps) with restraints on solute heavy atoms, (iii) a 12 ps simulation under an NPT ensemble at 10 K (thermostat relaxation = 0.1 ps) and pressure 1 atm (barostat relaxation = 50 ps) with restraints on solute heavy atoms, (iv) a 12 ps simulation under NPT ensemble at 300 K (thermostat relaxation = 0.1 ps) and pressure 1 atm (barostat relaxation = 50 ps) with restraints on solute heavy atoms, (v) a 24 ps simulation under NPT ensemble at 300 K (thermostat relaxation = 0.1 ps) and pressure 1 atm (barostat relaxation = 2 ps) with no restraints. A restraint force of 50 kcal mol^{-1} Å^2 was applied for all atomic restraints, and the target temperature and pressure were controlled by a Berendsen thermostat and barostat, respectively (Berendsen et al., 1981, 1984). For each protein-ligand system, the final production MD run was performed for 100 ns in the NPT ensemble at 300 K temperature (thermostat relaxation= 1 ps), and 1 atm pressure (barostat relaxation= 2 ps) using a Nose-Hoover thermostat and Martyna-Tobias-Klein barostat (Brańka, 2000; Martyna et al., 1994). The energy and trajectory of the production MD run was recorded at every 1.2 and 5 ps respectively. The trajectories were inspected in Maestro (Schrodinger, LLC, NY, USA) and an average structure was determined after refining by 2000 steps of steepest descent followed by conjugate gradient energy minimization. Each trajectory was analyzed for variations in root mean square deviation (RMSD), root mean square fluctuation (RMSF), the radius of gyration (Rg), solvent accessible surface area (SASA), total number of contacts, secondary structure variation, etc as described previously (Shamsi et al., 2019).

2.5. Free energy calculations using Prime MM-GBSA

The binding free energy of each protein-ligand complex was estimated using Prime module (Schrodinger, LLC, NY, USA) employing an MM-GBSA approach, as described previously (AlAjmi et al., 2018; Kumar Tripathi et al., 2013). In this approach, first the docked complexes were subjected to local optimization through molecular mechanics (MM) in Prime, and then their energies were minimized with an OPLS-AA (2005) force field with generalized Born surface area (GBSA) continuum solvent model. The binding free energy (ΔG_{Bind}) is estimated as (Kumar Tripathi et al., 2013):

$$\Delta G_{Bind} = \Delta E + \Delta G_{Solv} + \Delta G_{SA}$$
$$\Delta E = E_{Complex} - (E_{Protein} + E_{Ligand})$$

where, $E_{Complex}$, $E_{Protein}$, and E_{Ligand} are the respective values of minimized energies of protein-ligand complex, protein and ligand.

Table 2. Molecular docking parameters for drug-TACE interaction.

S. no.	Name of drug	Binding energy, ΔG (kcal mol^{-1})	Binding affinity, K_d (M^{-1})
1.	Control [3-{[4-(but-2-yn-1-yloxy) phenyl]sulfonyl} propane-1-thiol]	−7.3	2.26×10^5
2.	Acarbose	−7.5	3.17×10^5
3.	Bortezomib	nd	nd
4.	Budesonide	−6.2	3.53×10^4
5.	Capecitabine	−8.2	1.03×10^6
6.	Carboplatin	nd	nd
7.	**Celecoxib**	**−9.1**	**7.72×10^6**
8.	Ciclesonide	−7.6	3.75×10^5
9.	Cisplatin	nd	nd
10.	Cyclophosphamide	−5.2	6.52×10^3
11.	Diclofenac	−6.7	8.21×10^4
12.	Docetaxel	−7.7	4.44×10^5
13.	Donepezil	−8.0	7.37×10^5
14.	Doxorubicin	−8.1	8.73×10^5
15.	Epirubicin	−8.4	1.45×10^6
16.	Erlotinib	−7.9	6.23×10^5
17.	Exenatide	nd	nd
18.	Flunisolide	−6.0	2.52×10^4
19.	Fluorouracil	nd	nd
20.	Fluticasone	−6.1	2.98×10^4
21.	Fulvestrant	−8.3	1.22×10^6
22.	Galantamine	−6.4	4.94×10^4
23.	Glibenclamide	−8.2	1.03×10^6
24.	Gliclazide	−8.2	1.03×10^6
25.	Glimepiride	−8.0	7.37×10^5
26.	**Glipizide**	**−9.7**	**1.30×10^7**
27.	Glyclopyramide	−7.9	6.23×10^5
28.	Ibuprofen	−7.3	2.26×10^5
29.	Indomethacin	−7.5	3.17×10^5
30.	Insulin	nd	nd
31.	**Lapatinib**	**−9.4**	**7.84×10^6**
32.	Letrozole	−8.5	1.72×10^6
33.	Linagliptin	−7.1	1.61×10^5
34.	Liraglutide	nd	nd
35.	Mefenamic acid	−7.2	1.91×10^5
36.	Meloxicam	−8.0	7.37×10^5
37.	Memantine	−5.2	6.52×10^3
38.	Metformin	−5.0	4.65×10^3
39.	Naproxene	−8.2	1.03×10^6
40.	Paclitaxel	−6.9	1.15×10^5
41.	Pioglitazone	−7.5	3.17×10^5
42.	Repaglinide	−6.7	8.21×10^4
43.	Rivastigmine	−6.8	9.72×10^4
44.	Rosiglitazone	−8.5	1.72×10^6
45.	Saxagliptin	−6.9	1.15×10^5
46.	**Sitagliptin**	**−9.0**	**3.99×10^6**
47.	Sulindac	−7.6	3.75×10^5
48.	Tamoxifen	−7.1	1.61×10^5
49.	Toremifene	−6.9	1.15×10^5
50.	Vildagliptin	−6.4	4.94×10^4
51.	Vinorelbine	−6.1	2.98×10^4

Note. nd means not determined; drugs highlighted in bold were selected for molecular dynamics (MD) simulation.

$$\Delta G_{Sol} = G_{Solv\ (Complex)} - \left(G_{Solv\ (Protein)} + G_{Solv\ (Ligand)}\right)$$

where, $G_{Solv(Complex)}$, $G_{Solv(Protein)}$, and $G_{Solv(Ligand)}$ are the respective values of free energies of solvation of protein-ligand complex, protein and ligand.

$$\Delta G_{SA} = G_{SA\ (Complex)} - \left(G_{SA\ (Protein)} - G_{SA(Ligand)}\right)$$

where, $G_{SA(Complex)}$, $G_{SA(Protein)}$, and $G_{SA(Ligand)}$ are the respective values of surface area energies of protein-ligand complex, protein and ligand.

3. Results and discussion

3.1. Validation of molecular docking protocol

The authenticity of the molecular docking protocol adopted in this study was confirmed by re-docking the ligand in the X-ray crystal structure and computing the RMSDs between the re-docked pose and crystal structure pose (Figure 1). The all-atom RMSD of the ligand in re-docked and crystal structure poses was estimated to be 1.0245 Å, much lower than the acceptable limit of 2.0 Å.

3.2. Virtual screening of drugs for TACE binding

In this study, a total of 50 FDA-approved drugs commonly prescribed in Saudi Arabia for the treatment of chronic diseases were selected for their binding and hence inhibitory potential of the TACE enzyme. The binding energy and the corresponding binding affinity of drugs for the TACE enzyme are presented in Table 2. The binding energy of the control ligand was estimated to be −7.3 kcal mol^{-1}. Conversely, the binding energies of different drug molecules varied from

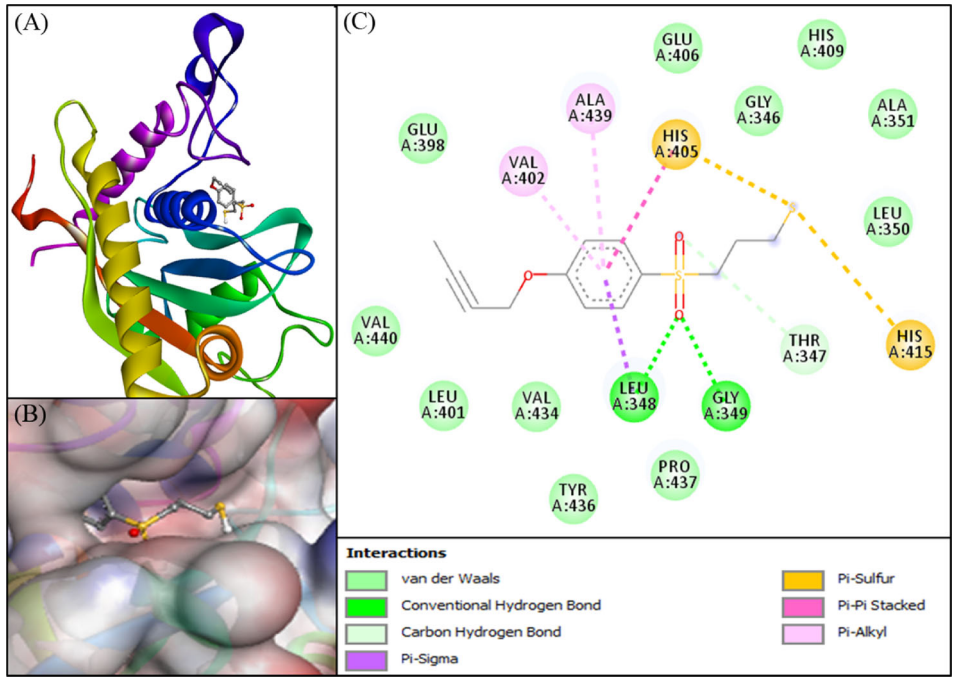

Figure 2. Molecular docking between TACE and control ligand [3-{[4-(but-2-yn-1-yloxy)phenyl]sulfonyl}propane-1-thiol], (A) Binding of control ligand at the active site of TACE, (B) 3 D representation of control ligand binding at the active site cavity of TACE, and (C) Molecular interaction and nature of forces involved in TACE-control ligand complex formation.

-5.0 kcal mol^{-1} to -9.4 kcal mol^{-1}. Drug molecules with the lowest binding energy and the highest binding affinity towards the TACE enzyme were Celecoxib, Glipizide, Lapatinib, and Sitagliptin. Binding energies of the shortlisted drug molecules, namely Celecoxib, Glipizide, Lapatinib, and Sitagliptin, were -9.1, -9.7, -9.4, and -9.0 kcal mol^{-1}, respectively.

3.3. Structure of TACE and its inhibition by control ligand

TACE or ADAM17 was discovered in 1997 as an enzyme responsible for the cleavage of membrane-bound tumor necrosis factor-α (TNF-α) into a soluble form (Black et al., 1997; Moss et al., 1997). TACE is expressed in different tissues such as the heart, kidney, brain, skeleton muscles, and its expression changes with time during embryonic development and adult life. It is a multi-domain protein of 824 amino acid residues, categorized into a signal sequence (1-17 aa), a prodomain (18-214 aa), a catalytic domain (215-473 aa) containing signature ZN^{2+} chelating HEXXHXXGXXH sequence spanning 405-415 aa, a disintegrin domain (474-572 aa), and a cytoplasmic domain (695-824 aa). The molecular docking of TACE with a thiol-based inhibitor, present in the X-ray crystal structure, as a control ligand revealed that it was bound at TACE's active site (Figure 2A,B). It formed two strong hydrogen bonds with Leu348:HN and Gly349:HN and one weak hydrogen bond with Thr347:CA. Also, there were two Pi-sulfur bonds between the control ligand and His405 and His415 of TACE. The TACE-control ligand complex was further stabilized by hydrophobic interactions with Val402, His405, Leu348, and Ala439 (Table 3). Several van der Waals' interactions were formed between the control ligand and Gly346, Leu350, Ala351, Glu398, Leu401, Glu406, His409, Val434, Tyr436, Pro437, and Val440 (Figure 2C). Binding energy and the corresponding binding affinity of the control ligand towards TACE were -7.3 kcal mol^{-1} and 2.26×10^5 M^{-1}, respectively.

3.4. Molecular docking analysis of shortlisted drugs

An insight into the molecular interaction between TACE and the shortlisted drug molecules was gained by analyzing their molecular docking poses (Figures 3–6 and Table 3).

Celecoxib is widely used as an anti-inflammatory drug in arthritis. It is a non-steroidal anti-inflammatory drug (NSAID) and inhibits the COX-2 enzyme explicitly. It is prescribed to treat pain and inflammation in osteoarthritis, acute pain, rheumatoid arthritis, ankylosing spondylitis, and juvenile rheumatoid arthritis (McCormack et al., 2011). The interaction between Celecoxib and TACE suggests that it binds at TACE's active site (Figure 3A,B). The TACE-Celecoxib complex was stabilized by six strong hydrogen bonds with Leu401:O, Glu406:OE2, Val434:O (two bonds), Val440:HN, and His495:NE2, and two weak hydrogen bonds with Leu350:CA and His415:CE1. The F-atom of Celecoxib formed five halogen bonds with Gly349:O (two bonds), Glu406:OE1, Glu406:OE2, and His415:NE2. Also, hydrophobic interactions between Celecoxib and Leu348, Val402, His405, His415, Ile438, and Ala439 (two bonds) further stabilized the TACE-Celecoxib complex (Table 3). Several van der Waals' interactions were also formed between Celecoxib and Gly346, Thr347, Ala351, Glu398, His409, and Tyr436 (Figure 3C). Celecoxib's binding energy for TACE was -9.1 kcal mol^{-1}, and binding affinity was 7.72×10^6 M^{-1}.

Table 3. Molecular docking parameters for drug-TACE interaction.

Drug	Donor-acceptor pair	Distance (Å)	Type of interaction
Control [3-{[4-(but-2-yn-1-yloxy) phenyl]sulfonyl} propane-1-thiol]	LEU348:HN - LIG:O	1.7654	Hydrogen bond
	GLY349:HN - LIG:O	2.2345	Hydrogen bond
	THR347:CA - LIG:O	3.7809	Carbon Hydrogen bond
	LEU348:CD1 - LIG	3.9989	Hydrophobic (Pi-Sigma)
	LIG:S - HIS405	5.3711	Pi-Sulfur
	LIG:S - HIS415	4.6125	Pi-Sulfur
	HIS405 - LIG	3.9042	Hydrophobic (Pi-Pi stacked)
	LIG - VAL402	4.9443	Hydrophobic (Pi-Alkyl)
	LIG - ALA439	4.5805	Hydrophobic (Pi-Alkyl)
Celecoxib	VAL440:HN - LIG:O	1.9305	Hydrogen bond
	LIG:HN - HIS405:NE2	2.6609	Hydrogen bond
	LIG:HN - GLU406:OE2	2.4561	Hydrogen bond
	LIG:H - VAL434:O	2.6535	Hydrogen bond
	LIG:H - LEU401:O	2.6783	Hydrogen bond
	LIG:H - VAL434:O	2.8753	Hydrogen bond
	LEU350:CA - LIG:F	3.3894	Carbon Hydrogen bond; Halogen bond
	HIS415:CE1 - LIG:F	3.2286	Carbon Hydrogen bond
	GLY349:O - LIG:F	3.1027	Halogen bond
	GLY349:O - LIG:F	3.1419	Halogen bond
	GLU406:OE1 - LIG:F	3.5144	Halogen bond
	GLU406:OE2 - LIG:F	3.2854	Halogen bond
	HIS415:NE2 - LIG:F	3.5573	Halogen bond
	HIS405 - LIG	3.8373	Hydrophobic (Pi-Pi stacked)
	HIS415 - LIG	5.3990	Hydrophobic (Pi-Pi T-shaped)
	LIG:C - ILE438	4.8338	Hydrophobic (Alkyl)
	LIG - LEU348	5.0959	Hydrophobic (Pi-Alkyl)
	LIG - VAL402	5.2812	Hydrophobic (Pi-Alkyl)
	LIG - ALA439	4.4810	Hydrophobic (Pi-Alkyl)
	LIG - ALA439	4.9123	Hydrophobic (Pi-Alkyl)
Glipizide	LEU348:HN - LIG:O	2.0494	Hydrogen bond
	ALA439:HN - LIG:O	2.0921	Hydrogen bond
	LIG:H - GLY346:O	2.0811	Hydrogen bond
	LIG:H - GLY346:O	2.0912	Hydrogen bond
	LIG:HN - GLU398:O	2.9178	Hydrogen bond
	LIG:C - VAL440:O	3.4424	Carbon hydrogen bond
	GLU398:OE2 - LIG	3.3921	Hydrophobic (Pi-Anion)
	LEU348:CD1 - LIG	3.7096	Hydrophobic (Pi-Sigma)
	LEU348:CD1 - LIG	3.5670	Hydrophobic (Pi-Sigma)
	HIS405 - LIG	4.2424	Hydrophobic (Pi-Pi stacked)
	ALA439 - LIG	5.4133	Hydrophobic (Alkyl)
	TYR390 - LIG	5.2472	Hydrophobic (Pi-Alkyl)
	LIG - VAL402	5.0567	Hydrophobic (Pi-Alkyl)
	LIG - ALA439	4.4743	Hydrophobic (Pi-Alkyl)
	LIG - ILE394	5.0621	Hydrophobic (Pi-Alkyl)
	LIG - ALA439	4.1730	Hydrophobic (Pi-Alkyl)
Lapatinib	ALA439:HN - LIG:O	2.6582	Hydrogen bond
	VAL440:HN - LIG:O	2.4171	Hydrogen bond
	LIG:H - GLY346:O	2.3288	Hydrogen bond
	ALA439:HN - LIG	3.0065	Pi-Donor Hydrogen bond
	LEU348:CD1 - LIG	3.9624	Hydrophobic (Pi-Sigma)
	ILE438:CG2 - LIG	3.8618	Hydrophobic (Pi-Sigma)
	TYR390 - LIG:Cl	5.1441	Hydrophobic (Pi-Alkyl)
	LIG - ALA439	4.9035	Hydrophobic (Pi-Alkyl)
	LIG - ALA439	4.5235	Hydrophobic (Pi-Alkyl)
	LIG - LYS392	4.5248	Hydrophobic (Pi-Alkyl)
	LIG - ALA439	4.4297	Hydrophobic (Pi-Alkyl)
Sitagliptin	VAL440:HN - LIG:F	2.4671	Hydrogen bond; Halogen bond
	LIG:HN - GLY346:O	2.1727	Hydrogen bond
	LIG:H - HIS415:NE2	2.9747	Hydrogen bond
	LIG:H - PRO437:O	2.0498	Hydrogen bond
	LEU401:O - LIG:F	3.1798	Halogen bond
	VAL434:O - LIG:F	3.4602	Halogen bond
	VAL434:O - LIG:F	3.0921	Halogen bond
	TYR436:O - LIG:F	3.3373	Halogen bond
	HIS405 - LIG	3.9730	Hydrophobic (Pi-Pi stacked)
	LIG - VAL402	5.3178	Hydrophobic (Pi-Alkyl)
	LIG - ALA439	4.3087	Hydrophobic (Pi-Alkyl)

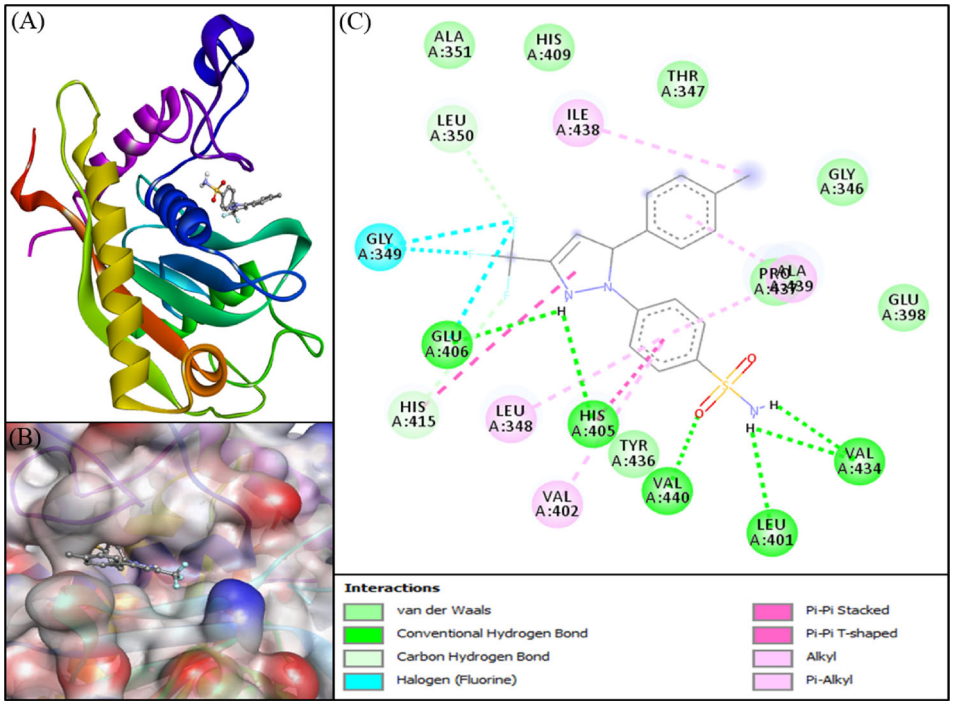

Figure 3. Molecular docking between TACE and Celecoxib. (A) Binding of Celecoxib at the active site of TACE, (B) 3 D representation of Celecoxib binding at the active site cavity of TACE, and (C) Molecular interaction and nature of forces involved in TACE-Celecoxib complex formation.

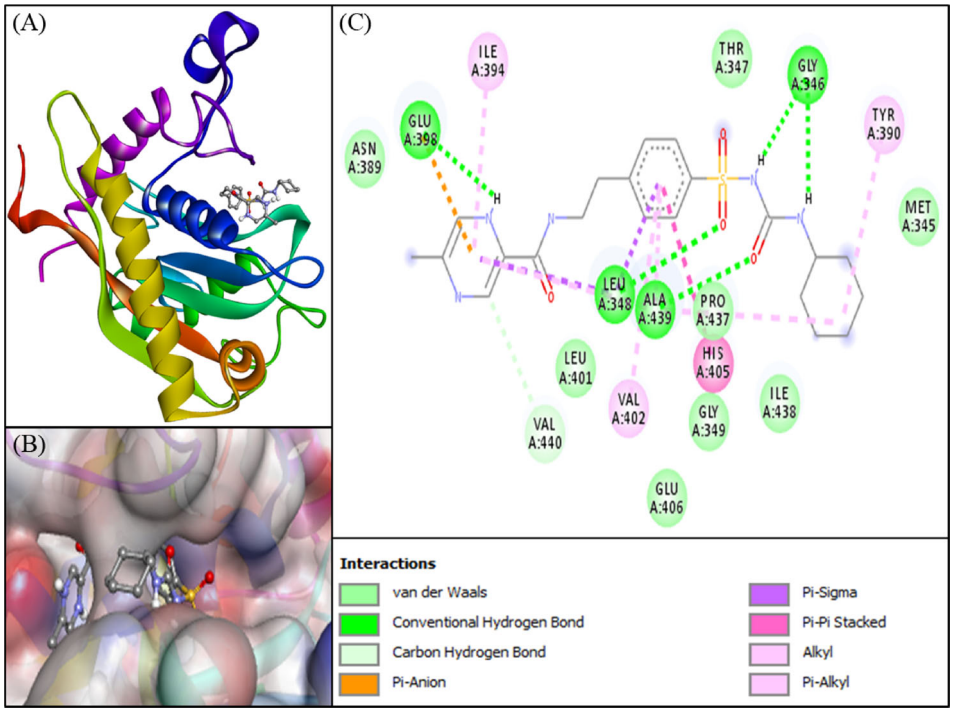

Figure 4. Molecular docking between TACE and Glipizide. (A) Binding of Glipizide at the active site of TACE, (B) 3 D representation of Glipizide binding at the active site cavity of TACE, and (C) Molecular interaction and nature of forces involved in TACE-Glipizide complex formation.

Glipizide is an antidiabetic drug of sulfonylurea class generally used in the treatment of type 2 diabetes. It acts by sensitizing the beta cells of the pancreatic islet of Langerhans to produce more insulin (Bösenberg & Van Zyl, 2008). Molecular docking between Glipizide and TACE indicates that it was bound at the active site of the enzyme (Figure 4A,B). The TACE-Glipizide complex was stabilized by five strong hydrogen bonds with Gly346:O (two bonds), Leu348:HN, Glu398:O, and Ala439:HN and one weak hydrogen bond with Val440:O. Glipizide also formed ten hydrophobic interactions with Leu348 (two bonds), Tyr390, Ile394, Glu398, Val402, His405, and Ala439 (three bonds) (Table 3). The TACE-Glipizide complex was further stabilized by several van der Waals' interactions formed between Glipizide and Met345, Thr347, Gly349, Asn389, Leu401, Glu406, Pro437, and Ile438 (Figure 4C). The binding energy of Glipizide for

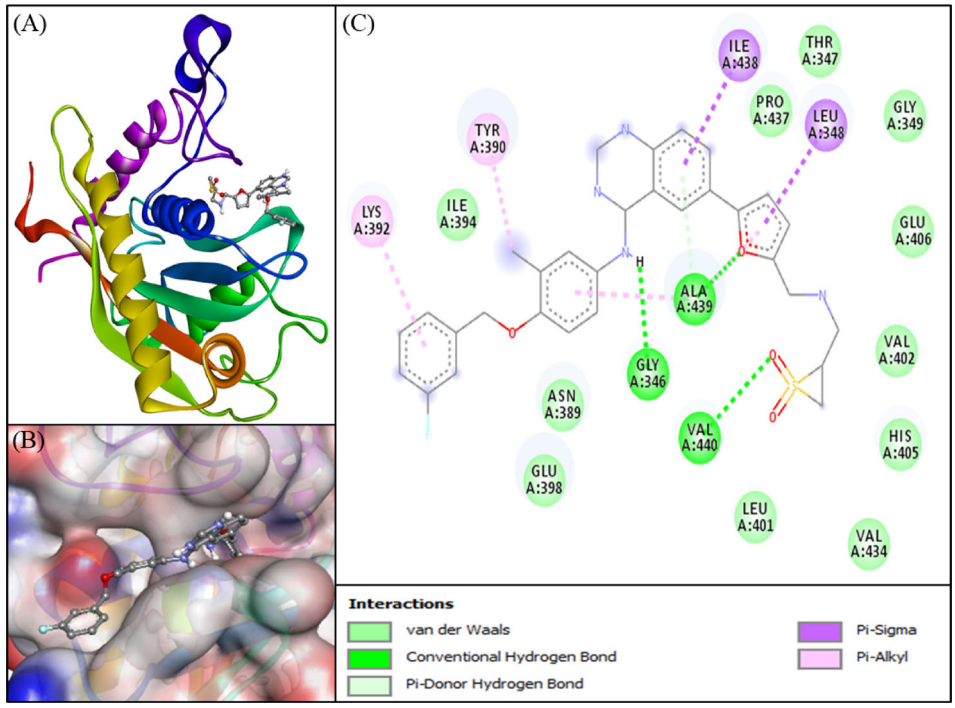

Figure 5. Molecular docking between TACE and Lapatinib. (A) Binding of Lapatinib at the active site of TACE, (B) 3 D representation of Lapatinib binding at the active site cavity of TACE, and (C) Molecular interaction and nature of forces involved in TACE-Lapatinib complex formation.

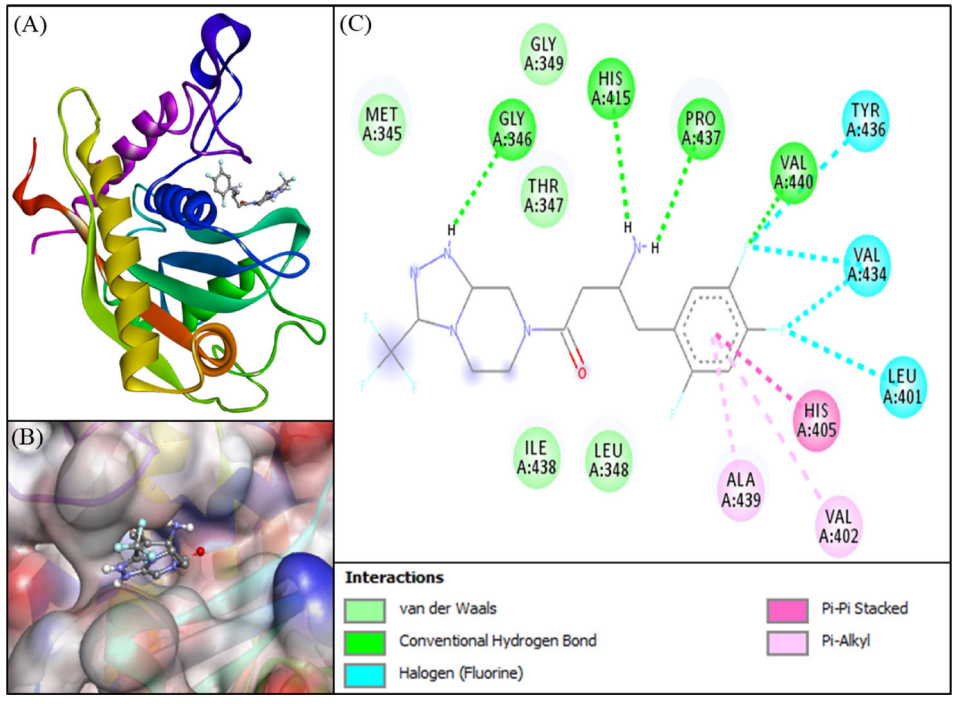

Figure 6. Molecular docking between TACE and Sitagliptin. (A) Binding of Sitagliptin at the active site of TACE, (B) 3 D representation of Sitagliptin binding at the active site cavity of TACE, and (C) Molecular interaction and nature of forces involved in TACE-Sitagliptin complex formation.

TACE was -9.7 kcal mol^{-1}, and binding affinity was $1.30 \times 10^{7}\ M^{-1}$.

Lapatinib is an orally active medication used to treat breast cancer and other tumors. It is a tyrosine kinase inhibitor that blocks HER2/neu and EGFR (epidermal growth factor receptor) pathways (Higa & Abraham, 2007; Wood et al., 2004). The interaction between Lapatinib and TACE indicates that the drug was bound at the active site of the enzyme (Figure 5A,B). The TACE-Lapatinib complex was stabilized by three strong hydrogen bonds with Gly346:O, Ala439:HN, and Val440:HN and one Pi-Donor hydrogen bond with Ala439:HN. In addition, Lapatinib formed seven hydrophobic interactions with Leu348, Tyr390, Lys392, Ile438, and Ala439 (three bonds) (Table 3). The TACE-Lapatinib interaction was

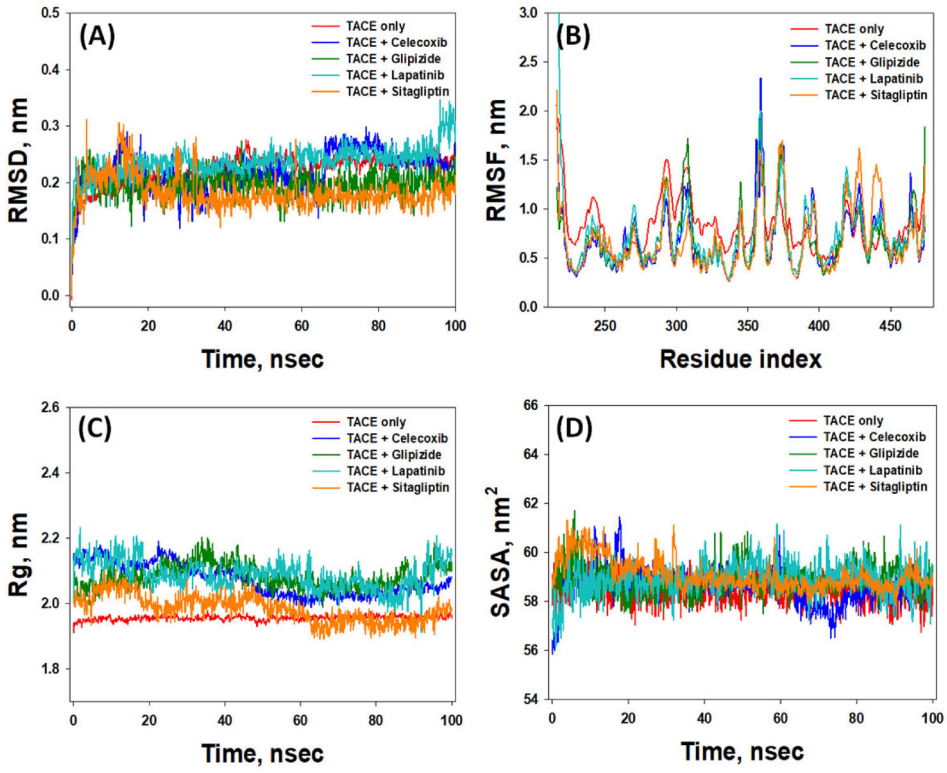

Figure 7. Molecular dynamics (MD) simulation of TACE in the absence or presence of different drug molecules. Dependency of (A) root mean square deviation (RMSD), (B) root mean square fluctuation (RMSF), (C) radius of Gyration (Rg), and (D) solvent accessible surface area (SASA) as a function of simulation.

Table 4. Average molecular dynamics (MD) parameters of TACE in the absence and presence of different drug molecules.

Protein-drug system	RMSD (nm)	Rg (nm)	SASA (nm^2)
TACE only	0.243 ± 0.08	1.95 ± 0.21	58.6 ± 1.8
TACE + Celecoxib	0.232 ± 0.06	2.06 ± 0.19	59.1 ± 3.2
TACE + Glipizide	0.201 ± 0.07	2.13 ± 0.26	59.5 ± 2.6
TACE + Lapatinib	0.255 ± 0.08	2.12 ± 0.28	59.3 ± 2.9
TACE + Sitagliptin	0.182 ± 0.09	1.98 ± 0.17	59.7 ± 3.1

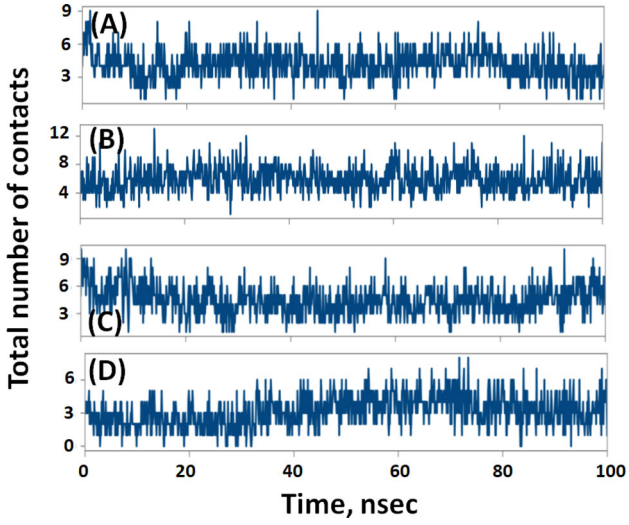

Figure 8. Variation in the total number of contacts formed between TACE and drugs. (A) Celecoxib, (B) Glipizide, (C) Lapatinib, and (D) Sitagliptin.

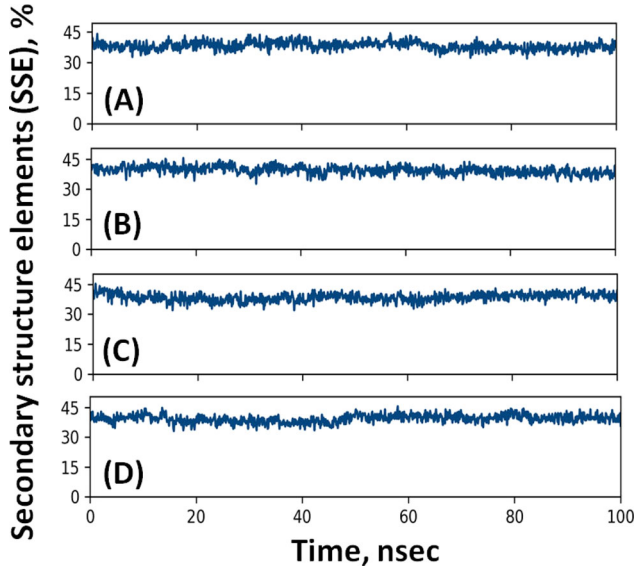

Figure 9. Variation in the secondary structure elements (SSE) of TACE when it formed complex with (A) Celecoxib, (B) Glipizide, (C) Lapatinib, and (D) Sitagliptin.

stabilized by several van der Waals' interactions formed with Thr347, Gly349, Asn389, Ile394, Glu398, Leu401, Val402, His405, Glu406, Val434, and Pro437 (Figure 5C). Lapatinib's binding energy for TACE was −9.4 kcal mol^{-1} and binding affinity was 7.84×10^6 M^{-1}.

Sitagliptin is also an antidiabetic drug used in the treatment of type 2 diabetes. It acts by inhibiting dipeptidyl peptidase-4 (DPP-4), increasing insulin production by sensitizing the pancreas' beta cells, and decreasing glucagon synthesis by the pancreas (Herman et al., 2005). Analysis of TACE-Sitagliptin interaction revealed that the drug was bound at the enzyme's active site (Figure 6A,B). The TACE-Sitagliptin complex was stabilized by four strong hydrogen bonds with

Gly346:O, His415:NE2, Val440:HN, and Pro437:O and five halogen bonds with Leu401:O, Val434:O (two bonds), Tyr436, and Val440:HN. In addition, Sitagliptin formed three hydrophobic interactions withVal402, His405 and Ala439 (three bonds) (Table 3). The TACE-Sitagliptin interaction was also stabilized by several van der Waals' interactions formed with Met345, Thr347, Gly349, Leu348, and Ile438 (Figure 6C). Sitagliptin's binding energy for TACE was -9.0 kcal mol^{-1}, and binding affinity was 3.99×10^6 M^{-1}.

3.5. Analysis of molecular dynamics (MD) simulation

TACE-drugs complexes' dynamics and stability were evaluated by performing molecular dynamics (MD) simulation under physiological conditions in triplicates (Figure 7 and Table 4). The initial frame of the TACE-drug complex was set as a reference, and the variation in root mean square deviation (RMSD) was monitored for 100 ns. The RMSD of a protein accounts for protein stability during the simulation. The RMSD of TACE alone fluctuated between 0.177 and 0.268 nm, with an average value of 0.243 ± 0.08 nm (Figure 7A). It indicated that the structure of TACE was not changed significantly during the simulation. The RMSDs of TACE-Celecoxib, TACE-Glipizide, TACE-Lapatinib, and TACE-Sitagliptin complexes were within 0.127–0.287 nm, 0.119–0.263 nm, 0.157–0.312 nm, and 0.134–0.306 nm, respectively. The average RMSD values of Celecoxib, Glipizide, Lapatinib, and Sitagliptin remained constant at 0.232 ± 0.06, 0.201 ± 0.07, 0.255 ± 0.08 and 0.182 ± 0.09 nm throughout the simulation (Table 4). There are many reports suggesting that a deviation 0.2 nm in RMSD is considered acceptable, as the difference is not significant (AlAjmi et al., 2018; Rehman et al., 2019).

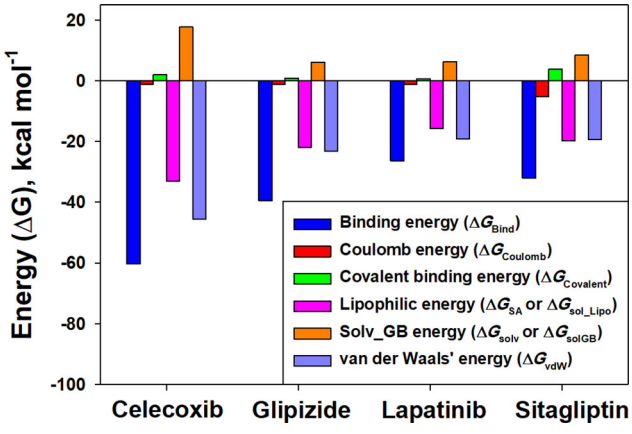

Figure 10. Free energy calculation of TACE-drugs interaction using Prime-MM/GBSA.

Thus, the results presented here confirmed the formation of a stable TACE-drug complex.

The root mean square fluctuation (RMSF) of a protein estimates the fluctuation in the protein's amino acid residues over the simulation time and can provide insight into the protein's overall conformational stability. RMSF of TACE alone and in complex with different drug molecules is given in Figure 7B. It is evident that the RMSF of TACE and TACE in complex with different drugs coincided, thus confirming that TACE's overall conformation remained conserved throughout the simulation.

Variation in a radius of gyration (Rg) and solvent accessible surface area (SASA) of a drug molecule as a function of simulation time indicates the protein-drug complex's overall compactness. The Rg of TACE alone remained constant throughout the simulation, with an average value of 1.95 ± 0.21 nm. Rg of TACE in the presence of Celecoxib, Glipizide, Lapatinib, and Sitagliptin fluctuated in the range of 2.10–2.18 nm, 2.01–2.19 nm, 1.98–2.22 nm, 1.96–2.08 nm, respectively (Figure 7C and Table 4). The average values of Rg for TACE-Celecoxib, TACE-Glipizide, TACE-Lapatinib, TACE-Sitagliptin complexes were 2.06 ± 0.19, 2.13 ± 0.26, 2.12 ± 0.28, and 1.98 ± 0.17 nm, respectively. Similarly, SASA of TACE alone remained constant and varied in the 57.2–59.8 nm^2 range with an average value of 58.6 ± 1.8 nm^2. SASA of TACE-Celecoxib, TACE-Glipizide, TACE-Lapatinib, TACE-Sitagliptin complexes varied in the range of 56.4–61.5 nm^2, 57.7–61.9 nm^2, 56.2–61.0 nm^2, and 58.1–61.2 nm^2 respectively, with average values of 59.1 ± 3.2, 59.5 ± 2.6, 59.3 ± 2.9 and 59.7 ± 3.1 nm^2 respectively (Figure 7D and Table 4). All these results confirmed that the studied drugs remain within TACE's binding cavity and form a stable TACE-drug complex.

3.6. Analysis of structural changes and contacts formed during MD simulation

We further analyzed whether the complex formed between TACE and the drugs was stable or not, by observing the number of contacts formed between them during MD simulation (Figure 8). We observed that during MD simulation, the total number of contacts TACE formed with Celecoxib, Glipizide, Lapatinib and Sitagliptin varied between 1-9, 3-13, 1-10, and 0-8 respectively. TACE formed an average of 5, 6, 5, and 3 contacts with Celecoxib, Glipizide, Lapatinib and Sitagliptin respectively. The results confirmed that all the drugs remained in the binding pocket of TACE and thus formed a stable complex throughout the simulation.

The interaction between a ligand and protein often leads to changes in protein's secondary structural elements (SSE) and thereby affect its stability. Thus, a check on the variation

Table 5. Free energy calculation of TACE-drug complexes using Prime/MM-GBSA.

	ΔE					
Drugs	$\Delta G_{Coulomb}$	ΔG_{vdW}	$\Delta G_{Covalent}$	ΔG_{Solv} or ΔG_{SolGB}	ΔG_{SA} or ΔG_{Sol_Lipo}	ΔG or ΔG_{Bind}
Celecoxib	−1.21	−45.65	1.97	17.63	−33.10	−60.36
Glipizide	−1.30	−23.15	0.87	6.10	−22.06	−39.54
Lapatinib	−1.25	−19.24	0.66	6.18	−15.81	−26.46
Sitagliptin	−5.23	−19.42	3.87	8.52	−19.73	−31.99

in SSE during the MD simulation is critical to overview the establishment of a stable complex between ligand and protein. In this study, we monitored the variation in total SSE (α-helix + β-sheet) of TACE in the presence of Celecoxib, Glipizide, Lapatinib and Sitagliptin during MD simulation (Figure 9). We found that the total SSE of TACE in complex with Celecoxib, Glipizide, Lapatinib and Sitagliptin was 38.25% (α-helix: 24.54% and β-sheets: 13.71%), 39.54% (α-helix: 25.91% and β-sheets: 13.63%), 38.48% (α-helix: 24.82% and β-sheets: 13.66%), and 39.38% (α-helix: 25.58% and β-sheets: 13.80%) respectively. It should be noted that the SSE of all protein-drug complexes remained consistent throughout the simulation, suggesting a stable conformation and thus a stable interaction between protein and drugs.

3.7. Analysis of Prime-MM/GBSA calculations

Prime-MM/GBSA is the most accurate parameter to evaluate the stability of protein-drug complexes. In this method, the effect of solvent on the overall stability of protein-drug complexes is also considered. Although, the free energy calculations are computationally demanding, the Prime-MM/GBSA scores are significantly correlated with the experimentally determined values. We have calculated the Prime-MM/GBSA of TACE in complex with the selected drugs namely Celecoxib, Glipizide, Lapatinib, and Sitagliptin (Figure 10 and Table 5). As evident from Table 5, Celecoxib has the lowest ΔG_{Bind} energy (–60.36 kcal mol^{-1}), followed by Glipizide (–39.54 kcal mol^{-1}), Sitagliptin (–31.99 kcal mol^{-1}), and Lapatinib (–26.46 kcal mol^{-1}). Principally, van der Waals' energy (ΔG_{vdW}) and non-polar solvation or lipophilic energy (ΔG_{SA} or ΔG_{Sol_Lipo}) contribute favorably towards the formation of a stable protein-drug complex, while covalent ($\Delta G_{Covalent}$) and solvation energies (ΔG_{Solv} or ΔG_{SolGB}) oppose a stable protein-drug complex.

All the energies are in kcal mol^{-1}. ΔE, $\Delta G_{Coulomb}$, ΔG_{vdW}, $\Delta G_{Covalent}$, ΔG_{Solv} or ΔG_{SolGB}, ΔG_{SA} or $\Delta G_{Sol\text{-}Lipo}$, and ΔG or ΔG_{Bind} stands for minimized energy, coulomb energy, covalent binding energy, solvation energy, lipophilic energy and binding energy, respectively.

4. Conclusion

The pathogenesis of SARS-CoV-2 includes the entry of virus particles into cells, and the formation of soluble ACE2 from membrane-bound ACE2 receptors. The overall process of SARS-CoV-2 binding to ACE2 and inducing TACE to shred ACE2 ectodomain is poorly understood. While soluble ACE2 may act as a pseudoreceptor to attract other virus particles, the reduced population of membrane-bound ACE2 receptors affects the Renin-Angiotensin pathway. Any imbalance in the homeostasis of Renin-Angiotensin pathways leads to severe inflammation and lung damage. In this study, the interaction between TACE or ADAM17 and FDA-approved drugs used to treat chronic diseases is studied using molecular docking and molecular dynamics simulation. We found that Celecoxib, Glipizide, Lapatinib and Sitagliptin are potential inhibitors of TACE. TACE is responsible for shedding membrane-bound ACE2 receptors into soluble ACE2 receptor. Thus, the inhibition of TACE would increase the population of membrane-bound ACE2 receptors, which may facilitate SARS-CoV-2 infection. Our hypothesis is well supported by the observation that the shedding of ACE2 has been blocked by other well-known active TACE inhibitors such as Marimastat, TAPI-0, TAPI-1, TAPI-2. The available TACE inhibitors are designed to inhibit the formation of TNFα. To the best of our knowledge, this is the first report which proposes the aggravation of SARS-CoV-2 infection in patients suffering from chronic diseases, due to the inhibition of TACE.

Acknowledgment

The authors acknowledge the generous support from Saudi Ministry of Health for funding this research under project no. 728 in April 14, 2020.

Disclosure statement

The authors declare no conflict of interest.

Funding

This work was funded by Ministry of Health, Saudi Arabia.

References

AlAjmi, M. F., Rehman, M. T., Hussain, A., & Rather, G. M. (2018). Pharmacoinformatics approach for the identification of Polo-like kinase-1 inhibitors from natural sources as anti-cancer agents. *International Journal of Biological Macromolecules*, *116*, 173–181. https://doi.org/10.1016/j.ijbiomac.2018.05.023

Al-Yousef, H. M., Ahmed, A. F., Al-Shabib, N. A., Laeeq, S., Khan, R. A., Rehman, M. T., Alsalme, A., Al-Ajmi, M. F., Khan, M. S., & Husain, F. M. (2017). Onion peel ethylacetate fraction and its derived constituent quercetin 40-O-β-D glucopyranoside attenuates quorum sensing regulated virulence and biofilm formation. *Frontiers in Microbiology*, *8*, 1675. https://doi.org/10.3389/fmicb.2017.01675

Bandarage, U. K., Wang, T., Come, J. H., Perola, E., Wei, Y., & Rao, B. G. (2008). Novel thiol-based TACE inhibitors. Part 2: Rational design, synthesis, and SAR of thiol-containing aryl sulfones. *Bioorganic & Medicinal Chemistry Letters*, *18*(1), 44–48. https://doi.org/10.1016/j.bmcl.2007.11.014

Berendsen, H. J. C., Postma, J. P. M., Van Gunsteren, W. F., Dinola, A., & Haak, J. R. (1984). Molecular dynamics with coupling to an external bath. *The Journal of Chemical Physics*, *81*(8), 3684–3690. https://doi.org/10.1063/1.448118

Berendsen, H. J. C., Postma, J. P. M., van Gunsteren, W. F., & Hermans, J. (1981). *Interaction models for water in relation to protein hydration*. In Pullman B. (Ed.), *Intermolecular forces. The Jerusalem Symposia on Quantum Chemistry and Biochemistry*, vol. 14. Dordrecht: Springer. https://doi.org/10.1007/978-94-015-7658-1_21

Black, R. A., Rauch, C. T., Kozlosky, C. J., Peschon, J. J., Slack, J. L., Wolfson, M. F., Castner, B. J., Stocking, K. L., Reddy, P., Srinivasan, S., Nelson, N., Boiani, N., Schooley, K. A., Gerhart, M., Davis, R., Fitzner, J. N., Johnson, R. S., Paxton, R. J., March, C. J., & Cerretti, D. P. (1997). A metalloproteinase disintegrin that releases tumour-necrosis factor-alpha from cells. *Nature*, *385*(6618), 729–733. https://doi.org/10.1038/385729a0

Bösenberg, L. H., & Van Zyl, D. G. (2008). The mechanism of action of oral antidiabetic drugs: A review of recent literature. *Journal of*

Endocrinology, Metabolism and Diabetes of South Africa, *13*(3), 80–89. https://doi.org/10.1080/22201009.2008.10872177

Brańka, A. C. (2000). Nosé-Hoover chain method for nonequilibrium molecular dynamics simulation. *Physical Review E*, *61*(5), 4769–4773. https://doi.org/10.1103/PhysRevE.61.4769

Gralinski, L. E., & Menachery, V. D. (2020). Return of the Coronavirus: 2019-nCoV. *Viruses*, *12*(2), 135. https://doi.org/10.3390/v12020135

Herman, G. A., Stevens, C., Van Dyck, K., Bergman, A., Yi, B., De Smet, M., Snyder, K., Hilliard, D., Tanen, M., Tanaka, W., Wang, A. Q., Zeng, W., Musson, D., Winchell, G., Davies, M. J., Ramael, S., Gottesdiener, K. M., & Wagner, J. A. (2005). Pharmacokinetics and pharmacodynamics of sitagliptin, an inhibitor of dipeptidyl peptidase IV, in healthy subjects: Results from two randomized, double-blind, placebo-controlled studies with single oral doses. *Clinical Pharmacology and Therapeutics*, *78*(6), 675–688. https://doi.org/10.1016/j.clpt.2005.09.002

Heurich, A., Hofmann-Winkler, H., Gierer, S., Liepold, T., Jahn, O., & Pohlmann, S. (2014). TMPRSS2 and ADAM17 cleave ACE2 differentially and only proteolysis by TMPRSS2 augments entry driven by the severe acute respiratory syndrome Coronavirus spike protein. *Journal of Virology*, *88*(2), 1293–1307. https://doi.org/10.1128/JVI.02202-13

Higa, G. M., & Abraham, J. (2007). Lapatinib in the treatment of breast cancer. *Expert Review of Anticancer Therapy*, *7*(9), 1183–1192. https://doi.org/10.1586/14737140.7.9.1183

Hoffmann, M., Kleine-Weber, H., Schroeder, S., Krüger, N., Herrler, T., Erichsen, S., Schiergens, T. S., Herrler, G., Wu, N.-H., Nitsche, A., Müller, M. A., Drosten, C., & Pöhlmann, S. (2020). SARS-CoV-2 cell entry depends on ACE2 and TMPRSS2 and is blocked by a clinically proven protease inhibitor. *Cell*, *181*(2), 271–280.e8. https://doi.org/10.1016/j.cell.2020.02.052

Khan, M. S., Qais, F. A., Rehman, M. T., Ismail, M. H., Alokail, M. S., Altwaijry, N., Alafaleq, N. O., AlAjmi, M. F., Salem, N., & Alqhatani, R. (2020). Mechanistic inhibition of non-enzymatic glycation and aldose reductase activity by naringenin: Binding, enzyme kinetics and molecular docking analysis. *International Journal of Biological Macromolecules*, *159*, 87–97. https://doi.org/10.1016/j.ijbiomac.2020.04.226

Kumar Tripathi, S., Muttineni, R., & Singh, S. K. (2013). Extra precision docking, free energy calculation and molecular dynamics simulation studies of CDK2 inhibitors. *Journal of Theoretical Biology*, *334*, 87–100. https://doi.org/10.1016/j.jtbi.2013.05.014

Lan, J., Ge, J., Yu, J., Shan, S., Zhou, H., Fan, S., Zhang, Q., Shi, X., Wang, Q., Zhang, L., & Wang, X. (2020). Structure of the SARS-CoV-2 spike receptor-binding domain bound to the ACE2 receptor. *Nature*, *581*(7807), 215–220. https://doi.org/10.1038/s41586-020-2180-5

Lu, R., Zhao, X., Li, J., Niu, P., Yang, B., Wu, H., Wang, W., Song, H., Huang, B., Zhu, N., Bi, Y., Ma, X., Zhan, F., Wang, L., Hu, T., Zhou, H., Hu, Z., Zhou, W., Zhao, L., … Tan, W. (2020). Genomic characterisation and epidemiology of 2019 novel coronavirus: Implications for virus origins and receptor binding. *The Lancet*, *395*(10224), 565–574. https://doi.org/10.1016/S0140-6736(20)30251-8

Luan, J., Lu, Y., Jin, X., & Zhang, L. (2020). Spike protein recognition of mammalian ACE2 predicts the host range and an optimized ACE2 for SARS-CoV-2 infection. *Biochemical and Biophysical Research Communications*, *526*(1), 165–169. https://doi.org/10.1016/j.bbrc.2020.03.047

Martyna, G. J., Tobias, D. J., & Klein, M. L. (1994). Constant pressure molecular dynamics algorithms. *The Journal of Chemical Physics*, *101*(5), 4177–4189. https://doi.org/10.1063/1.467468

McCormack, P. L., Lanas, A., McKenna, F., Patrignani, P., & Simon, L. S. (2011). Celecoxib: A review of its use for symptomatic relief in the treatment of osteoarthritis, rheumatoid arthritis and ankylosing spondylitis. *Drugs*, *71*(18), 2457–2489. https://doi.org/10.2165/11208240-000000000-00000

Monteil, V., Kwon, H., Prado, P., Hagelkrüys, A., Wimmer, R. A., Stahl, M., Leopoldi, A., Garreta, E., Hurtado Del Pozo, C., Prosper, F., Romero, J. P., Wirnsberger, G., Zhang, H., Slutsky, A. S., Conder, R., Montserrat, N., Mirazimi, A., & Penninger, J. M. (2020). Inhibition of SARS-CoV-2 infections in engineered human tissues using clinical-grade soluble human ACE2. *Cell*, *181*(4), 905–913.e7. https://doi.org/10.1016/j.cell.2020.04.004

Morris, G. M., Huey, R., Lindstrom, W., Sanner, M. F., Belew, R. K., Goodsell, D. S., & Olson, A. J. (2009). AutoDock4 and AutoDockTools4: Automated docking with selective receptor flexibility. *Journal of Computational Chemistry*, *30*(16), 2785–2791. https://doi.org/10.1002/jcc.21256

Moss, M. L., Jin, S. L., Milla, M. E., Bickett, D. M., Burkhart, W., Carter, H. L., Chen, W. J., Clay, W. C., Didsbury, J. R., Hassler, D., Hoffman, C. R., Kost, T. A., Lambert, M. H., Leesnitzer, M. A., McCauley, P., McGeehan, G., Mitchell, J., Moyer, M., Pahel, G., … Becherer, J. D. (1997). Cloning of a disintegrin metalloproteinase that processes precursor tumour-necrosis factor-alpha. *Nature*, *385*(6618), 733–736. https://doi.org/10.1038/385733a0

Palau, V., Riera, M., & Soler, M. J. (2020). ADAM17 inhibition may exert a protective effect on COVID-19. *Nephrology, Dialysis, Transplantation: Official Publication of the European Dialysis and Transplant Association - European Renal Association*, *35*(6), 1071–1072. https://doi.org/10.1093/ndt/gfaa093

Rabbani, N., Tabrez, S., Islam, B. U., Rehman, M. T., Alsenaidy, A. M., AlAjmi, M. F., Khan, R. A., Alsenaidy, M. A., & Khan, M. S. (2018). Characterization of colchicine binding with normal and glycated albumin: In vitro and molecular docking analysis. *Journal of Biomolecular Structure & Dynamics*, *36*(13), 3453–3462. https://doi.org/10.1080/07391102.2017.1389661

Rehman, M. T., Alajmi, M. F., Hussain, A., Rather, G. M., & Khan, M. A. (2019). High-throughput virtual screening, molecular dynamics simulation, and enzyme kinetics identified ZINC84525623 as a potential inhibitor of NDM-1. *International Journal of Molecular Sciences*, *20*(4), 819. https://doi.org/10.3390/ijms20040819

Rehman, M. T., Shamsi, H., & Khan, A. U. (2014). Insight into the binding mechanism of imipenem to human serum albumin by spectroscopic and computational approaches. *Molecular Pharmaceutics*, *11*(6), 1785–1797. https://doi.org/10.1021/mp500116c

Shamsi, A., Mohammad, T., Khan, M. S., Shahwan, M., Husain, F. M., Rehman, M. T., Hassan, M. I., Ahmad, F., & Islam, A. (2019). Unraveling binding mechanism of Alzheimer's drug rivastigmine tartrate with human transferrin: Molecular docking and multi-spectroscopic approach towards neurodegenerative diseases. *Biomolecules*, *9*(9), 495. https://doi.org/10.3390/biom9090495

She, J., Jiang, J., Ye, L., Hu, L., Bai, C., & Song, Y. (2020). 2019 novel coronavirus of pneumonia in Wuhan, China: Emerging attack and management strategies. *Clinical and Translational Medicine*, *9*(1), 17–19. https://doi.org/10.1186/s40169-020-00271-z

Solis, F. J., & Wets, R. J. B. (1981). Minimization by random search techniques. *Mathematics of Operations Research*, *6*(1), 19–30. https://doi.org/10.1287/moor.6.1.19

Wood, E. R., Truesdale, A. T., McDonald, O. B., Yuan, D., Hassell, A., Dickerson, S. H., Ellis, B., Pennisi, C., Horne, E., Lackey, K., Alligood, K. J., Rusnak, D. W., Gilmer, T. M., & Shewchuk, L. (2004). A unique structure for epidermal growth factor receptor bound to GW572016 (Lapatinib): Relationships among protein conformation, inhibitor off-rate, and receptor activity in tumor cells. *Cancer Research*, *64*(18), 6652–6659. https://doi.org/10.1158/0008-5472.CAN-04-1168

Wu, J., Deng, W., Li, S., & Yang, X. (2020). Advances in research on ACE2 as a receptor for 2019-nCoV. *Cellular and Molecular Life Sciences*, *1*, 3. https://doi.org/10.1007/s00018-020-03611-x

Zhou, P., Yang, X.-L., Wang, X.-G., Hu, B., Zhang, L., Zhang, W., Si, H.-R., Zhu, Y., Li, B., Huang, C.-L., Chen, H.-D., Chen, J., Luo, Y., Guo, H., Jiang, R.-D., Liu, M.-Q., Chen, Y., Shen, X.-R., Wang, X., … Shi, Z.-L. (2020). A pneumonia outbreak associated with a new coronavirus of probable bat origin. *Nature*, *579*(7798), 270–273. https://doi.org/10.1038/s41586-020-2012-7

Zipeto, D., Palmeira, J., da, F., Argañaraz, G. A., & Argañaraz, E. R. (2020). ACE2/ADAM17/TMPRSS2 interplay may be the main risk factor for COVID-19. *Frontiers in Immunology*, *11*, 576745. https://doi.org/10.3389/fimmu.2020.576745